

Analyst

Accepted Manuscript



This is an *Accepted Manuscript*, which has been through the Royal Society of Chemistry peer review process and has been accepted for publication.

Accepted Manuscripts are published online shortly after acceptance, before technical editing, formatting and proof reading. Using this free service, authors can make their results available to the community, in citable form, before we publish the edited article. We will replace this *Accepted Manuscript* with the edited and formatted *Advance Article* as soon as it is available.

You can find more information about *Accepted Manuscripts* in the [Information for Authors](#).

Please note that technical editing may introduce minor changes to the text and/or graphics, which may alter content. The journal's standard [Terms & Conditions](#) and the [Ethical guidelines](#) still apply. In no event shall the Royal Society of Chemistry be held responsible for any errors or omissions in this *Accepted Manuscript* or any consequences arising from the use of any information it contains.



Analyst

ARTICLE

Enhancement of Binding Kinetics on Affinity Substrates by Laser Point Heating Induced Transport

Bu Wang^a and Xuanhong Cheng^{*a, b}Received 00th January 20xx,
Accepted 00th January 20xxDOI: 10.1039/x0xx00000x
www.rsc.org/

Enhancing the time response and detection limit of affinity-binding based biosensors is an area of active research. For diffusion limited reactions, introducing active mass transport is an effective strategy to reduce the equilibration time and improve surface binding. Here, a laser is focused on the ceiling of a microchamber to generate point heating, which introduces natural advection and thermophoresis to promote mass transport to the reactive floor. We first used COMSOL simulation to study how the kinetics of ligand binding is influenced by the optothermal effect. Afterwards, binding of biotinylated nanoparticles to NeutrAvidin-treated substrates are quantitatively measured with and without laser heating. It is discovered that laser induced point heating reduces reaction half-life locally, and the reduction improves with the natural advection velocity. In addition, non-uniform ligand binding on the substrate is induced by the laser with predictable binding patterns. This optothermal strategy holds a promise to improve time-response and sensitivity of biosensor and microarrays.

1. Introduction

Promoting specific and efficient interactions between an analyte and an affinity surface is key to the performance of biosensors and microarrays.¹⁻⁵ Many microsensors utilize diffusion as the sole transport mechanism and analyte consumption by the surface reaction can dominate diffusive feeding, resulting in diffusion limited reactions and long equilibration time. This problem is particularly severe for the capture of viral particles, which have diameters on the order of 10 nm to 100 nm, leading to low diffusivity. For example, human simplex virus have a diameter of 200 nm and diffusivity of $\sim 10^{-12} \text{ m}^2/\text{s}$. It takes over one hour for the viral particles to diffuse 100 μm . In fact, Squires *et al.* found that surface capture of viral particles in a physiologically relevant concentration is almost always diffusion controlled.⁶ To overcome this limit and improve the equilibration time, various transport strategies have been devised. Continuous feeding is a popular option to replenish analyte near the capture bed.⁷⁻⁹ Squires *et al.* compared the performance characteristics of biosensors with and without tangential flow and found faster sensor saturation with continuous feeding.⁶ Yanik *et al.* studied analyte binding to a plasmonic sensor based on a nanohole and discovered flow would compensate reaction induced depletion zones and improving binding by 14 fold.¹⁰ However, continuous feeding generally consumes a lot of analyte. Alternatively, Hart *et al.* used AC electroosmosis to

introduce recirculation and observed an a reduction of reaction equilibration time by up to a factor of 6, along with enhancement of antibody binding up to 6.7 times on an IgG detector.¹¹ Sigurdson *et al.* obtained an order of magnitude increase of the binding rate on an antibody sensor by electrothermal stirring.¹² Dielectrophoresis has also been employed to direct the migration of biological species.¹³ However, these electrokinetic methods require patterned electrodes and risk potential electrochemical reactions at the electrode-solution interface. Enhanced mass transport and analyte accumulation has also been achieved using acoustic radiation pressure. This method offers the flexibility of instantly changing the accumulation location, but suffers from the requirement of elaborate device fabrication.¹⁴ Optical tweezers have been shown to enhance analyte concentration next to a biosensor by several orders of magnitude, but bionanoparticles often don't have sufficient refractive index difference from the surrounding solution for efficient tweezing.^{15, 16}

Recently, a number of researchers reported dramatic molecular accumulation in a solution driven by a temperature gradient.¹⁷⁻²⁰ Two active transport processes occur under the temperature gradient: recirculation by natural advection and thermophoresis of solutes along or against the temperature gradient. The accumulation factor is controllable by the Soret coefficient of the analyte, temperature gradient and reactor geometry.¹⁸ The phenomenon has been proposed as a plausible mechanism to explain the origin of life,^{17, 21} and has been used to study colloid interfacial thermodynamics and biomolecule interactions.²²⁻²⁴ Inspired by these studies, this work explores if a mild temperature gradient can enhance the binding kinetics on an affinity surface. Compared to other methods, temperature gradients can be imposed on a reaction chamber remotely, saving the effort to fabricate electrodes and actuators into the reactor. Furthermore, a mild

^a Department of Materials Science and Engineering, Lehigh University, Bethlehem, PA, 18015, USA.

^b Bioengineering Program, Lehigh University, Bethlehem, PA, 18015, USA.

* Address correspondence to xuc207@lehigh.edu; Tel: 610-758-2002; Fax: 610-758-4244

Electronic Supplementary Information (ESI) available: See DOI: 10.1039/x0xx00000x

temperature range of 0–37°C is compatible with biological samples.^{22, 25} Compared to continuous feeding of analyte, temperature gradients promote mass transport without wasting precious samples.

Various strategies have been implemented to create temperature gradients. Miniaturized vessels are often used to promote a strong gradient with a mild temperature variation. Mao *et al.* generated a linear temperature gradient across a microfluidic channel by placing it between hot and cold water reservoirs.²⁶ Guijt *et al.* used endothermic and exothermic reactions as the heat source and drain.²⁷ Joule heating has been shown to offer more precise spatial and temporal control of temperature.^{28, 29} However, device fabrication is complicated in these strategies. Recently, Braun and Libchaber reported the use of a focused laser to generate a radial temperature gradients in microchambers. This setup allows remote temperature control with precision spatial and temporal resolution, requires no fabrication in the microchamber itself and is compatible with *in situ* optical microscopy.^{20, 28} Given these advantages, we adopted point laser heating in a microchamber for transport enhancement and studied affinity binding on the functionalized floor. COMSOL simulations was used first to reveal the physical processes generated by point heating. Afterwards, the binding of biotinylated 200nm particles to NeutrAvidin-immobilized substrates were studied experimentally in one microchamber geometry to mimic the capture of herpes simplex virus by an affinity substrate, and to validate the computational results.^{30, 31}

2. Simulation

Two-dimensional simulations were performed using COMSOL Multiphysics software, a commercial finite element package (COMSOL Inc., Burlington, MA). For the simple case of surface reactions without a temperature gradient, the analyte diffusivity was set to be $1.4 \times 10^{-12} \text{ m}^2/\text{s}$, corresponding to diffusivity of 200nm nanoparticles used in the experiments. The density and viscosity parameters of water at 293 K were selected from the COMSOL materials library. Using the *Surface Reactions* module, surface binding was stimulated as a second-order reaction with a forward rate constant $k_f = 2 \times 10^5 \text{ m}^3/\text{mol} \cdot \text{s}$, a value corresponding to the biotin and NeutrAvidin interaction.³² The reverse rate constant for the NeutrAvidin-Biotin interaction is $4 \times 10^{-4} / \text{s}$, which is small and was neglected.³² The bulk concentration of analyte at $t = 0$ was 0.05 nM, and the density of surface binding sites at $t = 0$ was fixed at $1 \times 10^{-8} \text{ mol}/\text{m}^2$.³³

To simulate surface binding in microwells with a temperature gradient, the *Heat Transfer in Solids* module was used and temperature at the center of the microwell ceiling was set at 303 K. The sidewalls and floor of the microwell were set at room temperature of 293 K. Thermophoresis was simulated using codes from Braun *et al.* with the *Coefficient Form PDE* module.²⁰ The thermodiffusion coefficient for the analyte, D_T , was set at $7 \times 10^{-13} \text{ m}^2/\text{s} \cdot \text{K}$ according to the literature for polystyrene beads.¹⁸ The *Laminar Flow* module was used to simulate heat induced natural convection. Parameters (density, heat capacity, viscosity and thermal conductivity) of water were selected from the COMSOL

materials library. The surface reaction was set up the same way as described above using the *Surface Reactions* module.

In both simulation setups, mass flux at the boundaries were set to be zero except for the reaction surface where reacted bulk species became surface species.

3. Experimental

3.1 Experimental Setup

The experiments were carried out on a modified confocal microscope (Olympus, PA, Figure 1A). The microchamber has a dimension of $50 \mu\text{m} \times 5 \text{ mm} \times 5 \text{ mm}$, and is capped with a chromium coated coverslip.³⁴ An IR laser (1064 nm) was introduced above the sample and was focused on the ceiling. The temperature gradient was calibrated using 50 mM 2',7'-bis-(2-carboxyethyl)-5-(and-6)-carboxyfluorescein (BCECF, Life Technologies, CA) in a 10 mM Tris buffer (Sigma Aldrich, WI). The fluorescence intensity of BCECF drops by 2.8% in response to an increase of 1 K in temperature.^{17, 18, 34} The temperature calibration was carried out by changing the input laser power and recording the corresponding fluorescence intensity right below the ceiling as shown in Supplementary I: Temperature Calibration. Images in all experiments were processed by software FV-10-ASW (Olympus, PA) and analyzed by ImageJ (National Institutes of Health).

3.2 Microwell Fabrication and Surface Treatment

A mixture of PDMS prepolymer and curing agent at a weight ratio of 10:1 (Sylgard 184, Dow-Corning, MI) was spin-coated on a coverslip ($2'' \times 3''$, thickness #1, Ted Pella, CA) at 500 rpm for 5 min. The resulting PDMS film of 50 μm thickness was cured on the coverslips at 65–75 °C overnight, and a square hole was cut in PDMS to create a $50 \mu\text{m} \times 5 \text{ mm} \times 5 \text{ mm}$ reaction chamber.

To functionalize the floor of the microwell, the devices were activated by oxygen plasma and submerged sequentially in the following solutions: 4% (v/v) solution of 3-mercaptopropyl trimethoxysilane (Gelest, PA) in ethanol for 1 hour at room temperature, 0.01 $\mu\text{mol}/\text{mL}$ N-gamma-Maleimidobutyryl-oxysulfosuccinimide ester (GMBS, Pierce Protein, IL) in ethanol for 1 hour at room temperature, and finally 10 $\mu\text{g}/\text{mL}$ NeutrAvidin (Pierce Protein, IL) in phosphate buffered saline (PBS, Sigma Aldrich, WI) for at least 1 h at 4 °C. Immediately before use, the microwells were blocked by 1% (w/v) bovine serum albumin (BSA, Sigma Aldrich, WI) in PBS for at least 15 min and blot dry. The control devices were functionalized similarly except for 0 $\mu\text{g}/\text{mL}$ NeutrAvidin in PBS.

3.3 Calibration of Fluorescence Intensity from Surface Binding

Polystyrene nanoparticles (Life Technologies, CA) 200 nm in diameter and labelled by both AF488 and biotin were used in this work. The particles were suspended in deionized water, sonicated for 20 min in an ice water bath and used immediately. To yield a proper range of surface nanoparticles density for calibration, nanoparticles suspensions of 0.004, 0.013, 0.04, 0.13 and 0.4 nM were used. Two microliter of nanoparticles suspension was pipetted into the functionalized microwell, and the microwell was capped with a coverslip ($1'' \times 1''$, Fisher Scientific, PA). The surface of the coverslip in contact with the suspension was coated with 100 nm chromium to

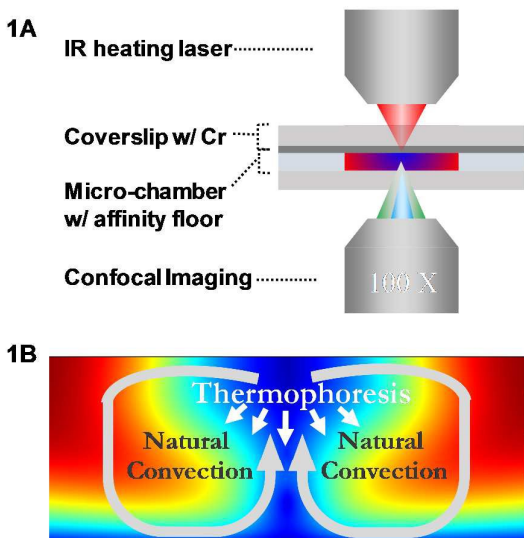


Figure 1: Schematic of the experimental setup and the active transport processes. (A) The experimental setup contains an IR laser focused on the ceiling of a microwell and a confocal microscope to image binding on the functionalized floor. (B) Point heating from the IR laser generates natural convection and thermophoresis, both of which promotes mass transport to the reactive floor. Color in the background is a simulated solute concentration profile in the bulk with point heating at the top center and depletion of the solute on the bottom substrate.

mimic the condition used in the temperature gradient experiments. The nanoparticle suspension was allowed to react in the microwell for 75 minutes and the fluorescence intensity on the microwell floor was recorded using a confocal microscope. Afterwards the microwell was washed 3 times with deionized water, air dried and coated with iridium for scanning electron microscope (SEM) imaging. The number of nanoparticles per unit area ($100 \mu\text{m}^2$) was counted from the SEM images. Non-specific binding was characterized using BSA passivated microwells without NeutrAvidin and nanoparticles at a concentration of 0.05 nM. For each condition, 3 samples were used for repeats; for each sample, 3 images were taken at random locations for both the fluorescence and SEM measurements. All data sets in graphs are presented as average \pm standard deviation from 9 data points.

3.4 Kinetics of Surface Binding without Temperature Gradients

To monitor the kinetics of surface binding without a temperature gradient, 2 μL of the nanoparticle suspension at 0.05 nM was allowed to react in a microwell covered by a chromium coated coverslip. The fluorescence intensity at the microwell floor was recorded every 5 minutes until the reaction reached a steady state. Then the average fluorescence intensity in each frame was converted to a surface concentration using the calibration curve described above. For each condition, 3-5 samples were used for repeats. All data sets in graphs are presented as average \pm standard deviation from at least 3 repeats.

3.5 Kinetics of Surface Binding with Temperature Gradients

To record the kinetics of surface binding with a temperature gradient, 2 μL of the nanoparticle suspension at 0.05 nM was pipetted into a functionalized microwell. Immediately after capping the microwell with a chromium-coated coverslip, an IR laser (1064nm) was focused on the chromium ceiling to generate local heating 10K above room temperature. The fluorescence intensity on the microwell floor was recorded every 5 min until the reaction reached a steady state. To analyze the resulting surface binding, radially distributed fluorescence intensity was measured. Since the fastest binding usually occurred at 50-100 μm from the center, fluorescence intensity from this region was averaged to obtain the binding kinetics. To verify that the measured fluorescence intensity was from surface binding rather than physical accumulation in the bulk, the heating laser was turned off after the reaction completed. The fluorescence intensity profile showed a minimal change, which confirmed that the particles were not free to diffuse anymore and were surface-bound. For each condition, 3-5 samples were used for repeats. All data sets in graphs are presented as average \pm standard deviation from at least 3 repeats.

4. Results and discussion

For a diffusion-controlled reactions, binding of the analyte to an affinity substrate can be extremely long. For example, for the surface capture of 200 nm particles at a concentration of 0.05 nM through the biotin-streptavidin interaction, the reaction half-life is on the order of hours when the height of the microwell exceeds 100 μm (Figure S2). To overcome the diffusion limit, focused laser is used to introduce point heating at the center of the microwell ceiling, which creates two active transport processes, natural advection and thermophoresis (Figure 1). Recirculation from natural convection replenishes the depletion zone near the surface. In addition, since most soft matter has a thermophobic behavior and migrate against the temperature gradient, the point heating drives nanoparticles towards the surface.

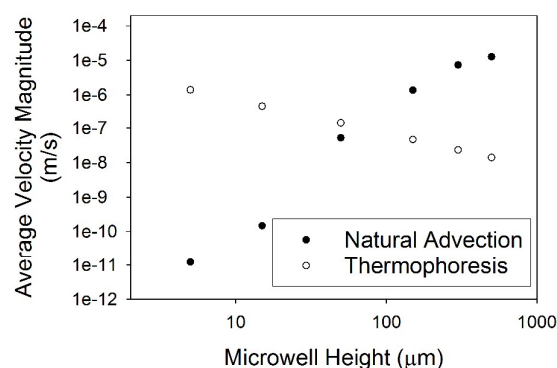


Figure 2: COMSOL simulation of average velocity magnitude from natural advection and thermophoresis in microwells with a fixed footprint footprint of $(500 \mu\text{m})^2$ and varied heights of 5 μm , 15 μm , 50 μm , 150 μm , 300 μm and 500 μm .

We first used COMSOL simulation to study the velocity of active transport as a function of the microchamber height. A temperature 10 K above the ambient temperature was introduced on the ceiling center. Footprint of the microchambers were all $(500 \mu\text{m})^2$ and the heights (H) were varied between $5 \mu\text{m}$ and $500 \mu\text{m}$. It is observed that the average velocity magnitude of natural convection increases drastically from $1.2 \times 10^{-11} \text{ m/s}$ to $1.3 \times 10^{-5} \text{ m/s}$ with the height (Figure 2). The thermophoretic velocity, which is equal to the product of thermal diffusion coefficient (D_T) and the temperature gradient, decreases from $2 \times 10^{-7} \text{ m/s}$ to $2 \times 10^{-9} \text{ m/s}$, assuming a linear temperature gradient between the heated ceiling center and the floor. The two active transport processes reach comparable velocities when the microwell height is $\sim 60 \mu\text{m}$, and advection dominates beyond $60 \mu\text{m}$.

To test the hypothesis that surface binding kinetics can be improved by point heating, COMSOL Multiphysics was used next to simulate the surface reaction of 200 nm biotinylated beads at 0.05 nM and a streptavidin functionalized substrate. Figure 3A shows the distribution of surface bound analyte in a $50 \mu\text{m}$ tall microwell at different time points. Surface binding is observed to be location dependent and a low binding zone is seen at the center. Faster binding occurs in the vicinity of the center than at locations far from the center. Figure 3B shows a snapshot of the simulated concentration distribution in bulk (top) and on the surface (bottom) 2 min after the reaction. The arrows in the top image of Figure 3B are velocity vectors from natural convection, indicating recirculation near the heat source. The non-uniform concentration in the bulk and on the surface results from a combined effect of thermophoresis,

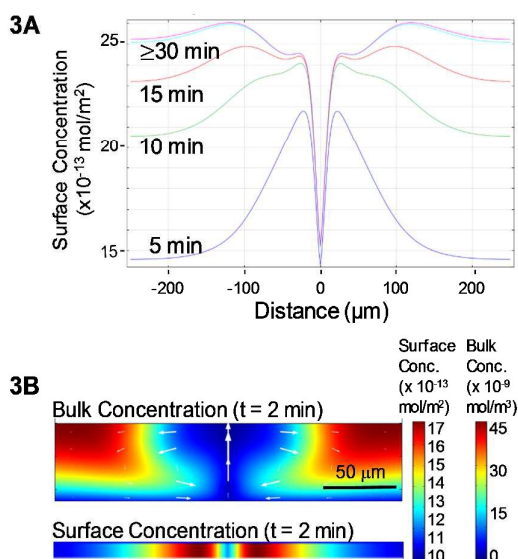


Figure 3: Simulated surface and bulk concentration in a $50 \mu\text{m}$ tall microwell with a 10 K temperature elevation at the top center. (A) Dynamic change of surface concentration as different distance from the center. (B) Bulk and surface concentrations 2 minutes after the reaction. A warmer color indicates a higher concentration. The white arrows in the top image are velocity vectors due to natural convection.

advection and surface reaction: (1) Thermophoresis pushes nanoparticles away from the heat source and towards the sides and bottom of the microwell. (2) Vortices generated by natural convection sweep nanoparticles on the microwell floor towards the center. While the fluid recirculates up near the center, the particles experience thermophoretic repulsion against the temperature gradient and remain near the center along the floor. (3) In the vicinity of the center where advection is the strongest, surface binding occurs quickly, which depletes analyte in this region. Afterwards, feeding into the central region is driven by diffusion, and binding slows down. At the same time, analyte is gradually captured on the surface far from the center, transported by diffusion mainly. The low capture zone at the center is a combined result of low advection and thermophobic migration.

Next, the reaction half-life was compared between heated and non-heated cases. In the cases with point heating, the half-life from the location of the greatest equilibrium binding was extracted from simulation, since the reaction kinetics is location dependent. As seen in Figure 4A, point heating

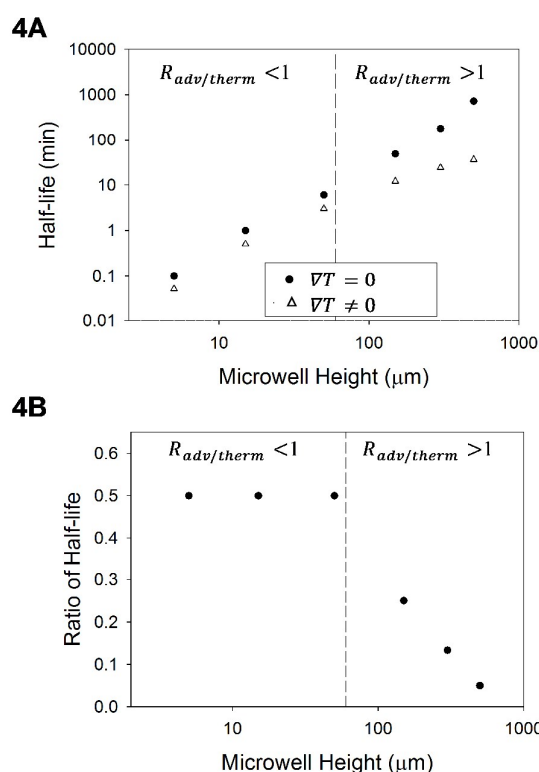


Figure 4: Simulated reaction half-life. Reaction constants corresponding to the NeutrAvidin-biotin pair were used. (A) Half-life of 200nm nanobeads reacting with affinity surfaces in microwells with ($\nabla T \neq 0$) and without ($\nabla T = 0$) point heating at the center of the ceiling. (B) The ratio of surface-reaction half-life (half-life with the temperature gradient divided by that without the temperature gradient) shows 50% reduction in the thermophoresis dominated region ($R_{adv/therm} < 1$). The ratio decreases with the chamber height in the advection dominated region ($R_{adv/therm} > 1$).

always reduces the binding half-life compared to reactions under a homogeneous temperature. The ratio of the half-life at different microchamber heights reveals two phases (Figure 4B). When thermophoretic velocity is greater than the average advection velocity, ($R_{\text{adv}}^{\text{therm}} < 1$, $H < 60\mu\text{m}$), the half-life is reduced by $\sim 50\%$ compared to reactions with a homogeneous temperature. This is a result of comparable fluxes by thermophoresis and diffusion. When advection dominates ($R_{\text{adv}}^{\text{therm}} \geq 1$, $H \geq 60\mu\text{m}$), reduction of the reaction half-life improves with the chamber height. In the $500\mu\text{m}$ tall microwell, the half-life is drastically reduced from 12 hrs to 36 min. Such a significant improvement of reaction rate is not surprising since the recirculation velocity is greater in tall microwells, creating stronger active transport.

The simulation results demonstrate that point heating improves the surface binding kinetics through enhanced transport. To verify the simulated findings, we next carried out experiments using 200 nm biotinylated nanoparticles and microwells with a dimension of $5\text{ mm} \times 5\text{ mm} \times 50\mu\text{m}$ and a NeutrAvidin treated floor. This height was selected since the steady state is reached relatively fast without heating to avoid photo-bleaching and evaporation.

To quantify the concentration of surface bound species dynamically, fluorescence intensity was measured in real time on the floor of microwells using confocal microscopy.^{20, 35-37} The intensity was converted to a surface concentration through a calibration curve in Figure 5. The calibration curve was generated by allowing nanoparticles of various concentrations (0.004 , 0.013 , 0.04 , 0.13 and 0.4 nM) to react in functionalized microwells for 75 min without laser heating, followed with measurements of fluorescence intensity on the microwell floor and SEM imaging of surface bound nanoparticle density. The reaction time is long enough to reach steady state in $50\mu\text{m}$ tall chambers. Control samples using 0.05 nM nanoparticles and BSA passivated microwells without NeutrAvidin was also tested to estimate nonspecific binding on the floor. As shown in Figure 5A, NeutrAvidin functionalized substrates promotes specific targets binding, which leads to a measurable increase of the fluorescence intensity. In Figure 5B, the fluorescence intensity shows a linear regression towards the surface concentration of nanoparticles with good correlation ($R^2 = 0.9915$). For later experiments, 0.05 nM nanoparticles were used to make sure the density of surface bound targets is well within the linear detection range.

Next we examined the surface binding kinetics in NeutrAvidin-functionalized microwells with and without laser heating. The laser generated a temperature 10 K higher than the ambient, confirmed ahead by BCECF fluorescence intensity measurements. The fluorescence intensity on the microwell floor due to nanoparticle binding was recorded every 5 min . The calibration curve in Figure 5 was used to convert the intensity to a surface concentration. Figure 6A shows a typical image with point heating 25 min after surface binding. The temperature gradient produces a low binding zone in the center, consistent with the simulation prediction in Figure 3. The radially distributed fluorescence intensity was measured every 5 minutes and the intensity in the region $50\text{-}100\mu\text{m}$ from the center was averaged to obtain the surface concentration. For comparison, the dynamic change of the surface fluorescence was also measured in microchambers

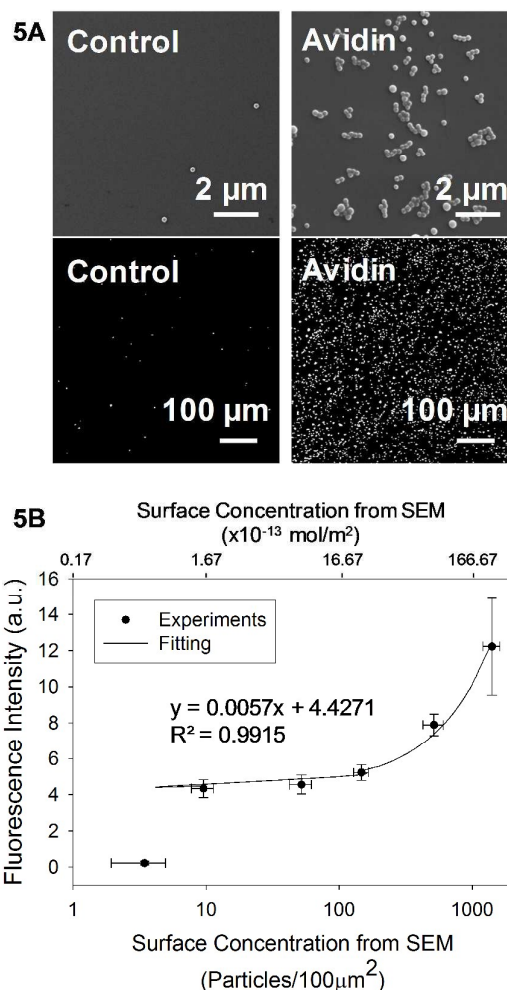


Figure 5: Calibration of the fluorescence intensity. A range of surface concentrations of nanoparticles were produced by reactions of nanoparticles at various concentrations with NeutrAvidin treated surfaces in microwells. The control was microwells with BSA passivation but no NeutrAvidin treatment. (A) Considerable difference is observed in both SEM images (top panel) and fluorescence intensity (bottom panel) when 0.05 nM nanoparticles reacted in a control microwell versus a NeutrAvidin-treated microwell. (B) The fluorescence intensity shows a linear regression towards the surface concentration of nanoparticles with $R^2 = 0.9915$. The error bars represent one standard deviation ($n=9$).

without point heating. As shown in Figure 6B, the measured surface concentration (dots) well matches the simulated kinetics at a distance of $100\mu\text{m}$ (lines). The half-life with point heating is ~ 3 minutes, versus ~ 6 minutes for the no-heating case. The steady-state surface binding with point heating is $\sim 5\%$ higher than without heating. But this improvement is not statistically significant, due to experimental variation of the same level.

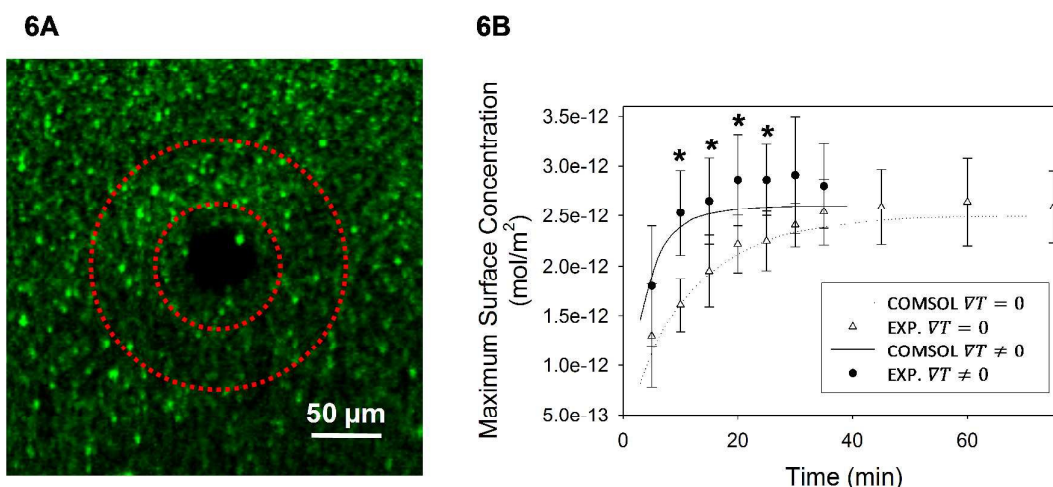


Figure 6: Experimental measurements of surface binding with a temperature gradient or under a homogenous temperature. (A) A typical fluorescence image 25 min after the reaction on the microwell floor when ∇T is present. (B) Kinetics of surface binding with (black dot) and without (empty triangle) temperature gradients measured from the ring region (50-100 μm from the center) in 6A. Radially averaged fluorescence intensity was used and 3-5 different samples were tested. The error bars represent one standard deviation ($n \geq 3$). The solid line is from simulated reactions with a temperature gradient and dash line from simulated reactions with a uniform temperature. The experimental results are in good agreement with the prediction from COMSOL simulation. Statistically different data points in reactions with and without temperature gradients are labelled with "*" ($p < 0.05$ by two-tailed student t test).

Several groups have reported non-uniform bulk accumulation induced by a mild temperature gradient.^{18, 20} Here, we demonstrate that surface binding kinetics can also be enhanced by the optothermal effect. Although the improvement of steady-state surface binding appears only moderate using the fast NeutrAvidin and biotin interaction, combining a temperature gradient with a patterned affinity substrate is expected to limit analyte depletion out of the affinity region and promote significantly greater local binding at a fast speed. This approach is especially appealing for micro- and nanosensors where diffusive transport of analyte to a miniaturized binding area is unrealistically long in a dilute solution.^{6, 38, 39} As a moderate temperature gradient is biocompatible and can be superposed on a microchamber remotely, it has the potential to be integrated with micro- and nanosensors without added complexity to the sensors themselves. The mild temperature elevation and a small heating volume on the order of nanoliter or less don't cause formation of undissolved air. It is also highly plausible to array the laser heating source for microarray applications.

5. Conclusions

In conclusion, using a focused laser to introduce a mild temperature gradient in a microwell reactor enhances mass transport and promotes surface binding kinetics. COMSOL simulation show that the enhanced transport is due to combined effects of thermophoresis and natural advection, and the relative contribution of each process is dependent on the microwell dimension. The benefits to the binding kinetics increases with the microchamber height. The simulation prediction is confirmed experimentally with one selected microwell geometry. The strategy to enhance surface binding

through a temperature gradient can be applied to improve the sensitivity and time response of biosensors and microarrays.

Acknowledgements

Funding for the research is provided by National Science Foundation under Grant No. 1014957. The authors also acknowledge Dr. Ou-Yang, Dr. Steven Ming-Tzo Wei, Dr. Jinxin Fu, Dr. Yi Hu and Chao Zhao for generously sharing their knowledge of optical physics.

Notes and references

- G. Mehta, K. Mehta, D. Sud, J. W. Song, T. Bersano-Begey, N. Futai, Y. S. Heo, M.-A. Mycek, J. J. Linderman and S. Takayama, *Biomed. Microdevices*, 2007, **9**, 123-134.
- W. Kusnezow, Y. V. Syagailo, I. Goychuk, J. D. Hoheisel and D. G. Wild, *Expert Rev. Mol. Diagn.*, 2006, **6**, 111-124.
- A. Bange, H. B. Halsall and W. R. Heineman, *Biosens. Bioelectron.*, 2005, **20**, 2488-2503.
- K. Sato, A. Hibara, M. Tokeshi, H. Hisamoto and T. Kitamori, *Adv. Drug Deliv. Rev.*, 2003, **55**, 379-391.
- T. Porstmann and S. T. Kiessig, *J. Immunol. Methods*, 1992, **150**, 5-21.
- T. M. Squires, R. J. Messinger and S. R. Manalis, *Nat. Biotechnol.*, 2008, **26**, 417-426.
- K. N. Han, C. A. Li and G. H. Seong, in *Annual Review of Analytical Chemistry, Vol 6*, Editon edn., 2013, vol. 6, pp. 119-141.
- D. Brennan, J. Justice, B. Corbett, T. McCarthy and P. Galvin, *Anal. Bioanal. Chem.*, 2009, **395**, 621-636.

- 1
2
3
4
5
6
7
8
9
10
11
12
13
14
15
16
17
18
19
20
21
22
23
24
25
26
27
28
29
30
31
32
33
34
35
36
37
38
39
40
41
42
43
44
45
46
47
48
49
50
51
52
53
54
55
56
57
58
59
60
9. B. Wang, A. L. Weldon, P. Kumnorkaew, B. Xu, J. F. Gilchrist and X. H. Cheng, *Langmuir*, 2011, **27**, 11229-11237.
10. A. A. Yanik, M. Huang, A. Artar, T. Y. Chang and H. Altug, *Appl. Phys. Lett.*, 2010, **96**, 021101.
11. R. Hart, R. Lec and H. M. Noh, *Sens. Actuator B-Chem.*, 2010, **147**, 366-375.
12. M. Sigurdson, D. Z. Wang and C. D. Meinhart, *Lab Chip*, 2005, **5**, 1366-1373.
13. R. Pethig, *Biomicrofluidics*, 2010, **4**, 35.
14. T. Kozuka, T. Tuziuti, H. Mitome and T. Fukuda, *Jpn. J. Appl. Phys. Part 1 - Regul. Pap. Short Notes Rev. Pap.*, 1998, **37**, 2974-2978.
15. A. Jonas and P. Zemanek, *Electrophoresis*, 2008, **29**, 4813-4851.
16. Y. Hu, X. Cheng and D. Ou-yang, *Biomedical Optics Express*, 2013, **4**, 1646-1653.
17. P. Baaske, F. M. Weinert, S. Duhr, K. H. Lemke, M. J. Russell and D. Braun, *Proc. Natl. Acad. Sci. U. S. A.*, 2007, **104**, 9346-9351.
18. S. Duhr and D. Braun, *Proc. Natl. Acad. Sci. U. S. A.*, 2006, **103**, 19678-19682.
19. S. Duhr and D. Braun, *Phys. Rev. Lett.*, 2006, **97**, 038103.
20. D. Braun and A. Libchaber, *Phys. Rev. Lett.*, 2002, **89**, 188103_188101-188103_188104.
21. D. Braun and A. Libchaber, *Phys. Biol.*, 2004, **1**, 1-8.
22. E. C. Gaffarogullari, A. Krause, J. Balbo, D. P. Herten and A. Jaschke, *RNA Biol.*, 2013, **10**, 1815-1821.
23. Y. X. Mao, L. L. Yu, R. Yang, L. B. Qu and P. D. Harrington, *Talanta*, 2015, **132**, 894-901.
24. J. A. Martin, J. L. Chavez, Y. Chushak, R. R. Chapleau, J. Hagen and N. Kelley-Loughnane, *Anal. Bioanal. Chem.*, 2014, **406**, 4637-4647.
25. C. J. Wienken, P. Baaske, U. Rothbauer, D. Braun and S. Duhr, *Nature Communications*, 2010, **1**, 7.
26. H. B. Mao, T. L. Yang and P. S. Cremer, *J. Am. Chem. Soc.*, 2002, **124**, 4432-4435.
27. R. M. Guijt, A. Dodge, G. W. K. van Dedem, N. F. de Rooij and E. Verpoorte, *Lab Chip*, 2003, **3**, 1-4.
28. V. Miralles, A. Huerre, F. Malloggi and M.-C. Jullien, *Diagnostics*, 2013, **3**, 33.
29. D. Vigolo, R. Rusconi, R. Piazza and H. A. Stone, *Lab Chip*, 2010, **10**, 795-798.
30. W. W. Zhong, *Anal. Bioanal. Chem.*, 2009, **394**, 47-59.
31. K. Sato, M. Sawayanagi, K. Hosokawa and M. Maeda, *Anal. Sci.*, 2004, **20**, 893-894.
32. J. R. Wayment and J. M. Harris, *Anal. Chem.*, 2009, **81**, 336-342.
33. J. J. Figueroa, University of South Florida, 2013.
34. C. Zhao, J. X. Fu, A. Oztekin and X. H. Cheng, *J. Nanopart. Res.*, 2014, **16**, 2625_2621-2611.
35. L. Y. Wang, X. W. Kan, M. C. Zhang, C. Q. Zhu and L. Wang, *Analyst*, 2002, **127**, 1531-1534.
36. Z. L. Jiang, W. E. Yuan and H. C. Pan, *Spectroc. Acta Pt. A-Molec. Biomolec. Spectr.*, 2005, **61**, 2488-2494.
37. H. Wang, Y. B. Li and M. Slavik, *J Rapid Methods Autom. Microbiol.*, 2007, **15**, 67-76.
38. C. C. Lin, J. H. Wang, H. W. Wu and G. B. Lee, *Journal of the Association for Laboratory Automation*, 2010, **15**, 253-274.
39. P. E. Sheehan and L. J. Whitman, *Nano Lett.*, 2005, **5**, 803-807.